



Article

Unprecedented Proline-Based Heterogeneous Organocatalyst for Selective Production of Vanillin

Farveh Saberi ^{1,2}, Daily Rodriguez-Padrón ², Araceli Garcia ² , Hamid Reza Shaterian ^{1,*} and Rafael Luque ^{2,3,*} 

¹ Department of Chemistry, Faculty of Sciences, University of Sistan and Baluchestan, Zahedan 98135-674, Iran; farveh.saberilemraski@gmail.com

² Departamento de Química Orgánica Universidad de Córdoba Campus de Rabanales, Edificio Marie Curie, Ctra N. IV-A, Km 396, 14014 Córdoba, Spain; dailydggs@gmail.com (D.R.-P.); qo2ganua@uco.es (A.G.)

³ Peoples Friendship University of Russia (RUDN University), 6 Miklukho-Maklaya str., 117198 Moscow, Russia

* Correspondence: hrshaterian@hamoon.usb.ac.ir (H.R.S.); rafael.luque@uco.es (R.L.)

Received: 3 April 2018; Accepted: 17 April 2018; Published: 20 April 2018



Abstract: An organocatalytic system based on an unprecedented proline analogue and iron oxide magnetic nanoparticles (Prn/Fe₂O₃@SiO₂) was designed and employed in vanillin production from isoeugenol and vanillyl alcohol. Full characterization of the obtained catalyst revealed the successful functionalization of the nanoparticle surface with the organic moieties. The activity of the magnetic bifunctional material was compared with its proton-unexchanged counterpart. Interestingly, the oxidation of isoeugenol resulted in being highly dependent on the acidic functionalities of the organocatalyst. Nonetheless, the catalytic performance of the proton-unexchanged catalyst suggested that the acidic and basic sites of the Prn/Fe₂O₃@SiO₂ exhibited a synergic effect, giving rise to higher conversion and selectivity. The presence of bifunctional groups in the proline analogue, together with the magnetic properties of the iron oxide nanoparticles, could lead to high efficiency, versatility, recoverability, and reusability.

Keywords: vanillyl alcohol; isoeugenol; organocatalyst; vanillin; magnetic core-shell

1. Introduction

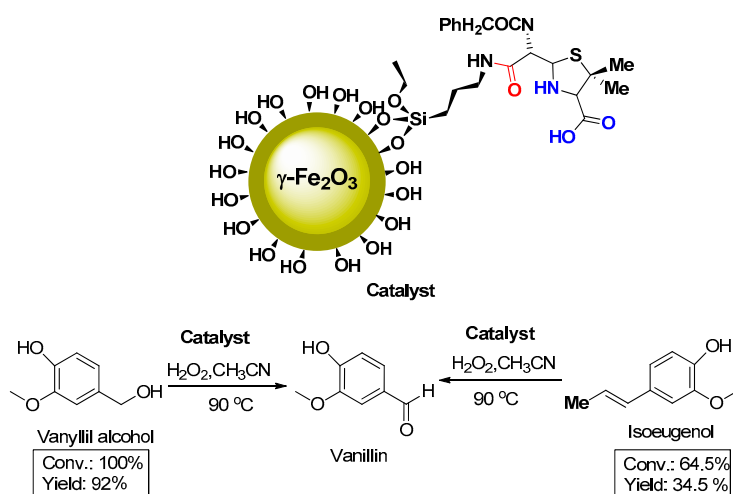
Valorization of lignocellulosic biomass has become an attractive approach for the production of added value chemicals and fuels, decreasing as well, environmental problems related to agricultural residues. Lignocellulosic biomass is typically composed by three main constituents: cellulose, hemicellulose, and lignin. In particular, lignin is a highly functionalized aromatic compound, which could lead to the design of outstanding chemical platforms. In this sense, vanillin is one of the most preeminent molecules, which can be obtained from lignin derived compounds such as eugenol, isoeugenol, and ferulic acid via oxidation pathways [1]. Synthetic vanillin is commonly used as flavoring agent in food, cosmetic, pharmaceutical, and fine chemical industries. Nowadays, this molecule is mainly produced from petro-based intermediates, predominantly glyoxylic acid and guaiacol, employing non-sustainable synthetic methodologies such as Riedel process [2]. Although synthesis of vanillin has been explored for many years, much more effort should still be devoted to excavating facile an environmentally-friendly protocols for the catalytic oxidation of lignin model compounds using cost effective organo-catalytic based technologies.

Vanillin synthesis from isoeugenol and vanillyl alcohol should be further investigated in order to find new alternatives to the conventional oxidation methods that require stoichiometric amounts of inorganic oxidants such as potassium permanganate, which are highly toxic and polluting [3].

In order to minimize chemical waste, the scientific community is moving towards the use of green oxidants including, H_2O_2 [4,5] and molecular oxygen [6]. In addition, the inherent arduous separation and recovery of homogeneous catalysts have led to the development of heterogeneous systems, as a priority of research activity in the green chemistry field. Thus, the use of clean oxidants and heterogeneous catalytic systems, open new possibilities to further develop environmentally friendly catalyzed processes [7,8]. In this regard, supported iron oxide nanoparticles has been reported to convert the isoeugenol to vanillin using H_2O_2 [9].

Moreover, the use of heterogeneous catalytic systems usually requires a filtration or centrifugation step to recover the catalyst. In this regard, magnetic nanoparticles (MNPs) has attracted a great interest since they can be easily separated from the reaction mixture by using a magnetic external field and reused for several cycles [10–12]. Nonetheless, maintaining the stability of these particles for a long time without agglomeration or precipitation is still a challenge [13,14]. Aiming to stabilize MNPs, several strategies have been proposed, such as coating or encapsulation in the form of core–shell structures or nanocomposites [15]. In particular, core–shell frameworks composed of $\gamma\text{-Fe}_2\text{O}_3$ and silica ($\gamma\text{-Fe}_2\text{O}_3@\text{SiO}_2$) are one of the most stable and efficient reported nanostructure for catalysis. Silica surface can be easily post-modified with a wide variety of catalytic species by using different organosiloxane precursors [16,17].

Functionalization of $\gamma\text{-Fe}_2\text{O}_3@\text{SiO}_2$ with organocatalysts could represent significant progress in the field of catalysis [18–20]. So far, many organocatalysts have been developed based on their carboxylic and amine functionalities, which could play a crucial role in the catalytic reaction [21–23]. Particularly, proline is an amino acid which contains α -amino and α -carboxylic acid groups [24,25]. Proline and its derivatives have been used as asymmetric catalysts in proline organocatalysis reactions [26], including aldol reaction [27], Knoevenagel [28], and multicomponent reaction [29]. To the far of our knowledge, the preparation of proline based solid-supported organocatalysts commonly requires several reaction steps and non-environmentally friendly procedures [30]. Although organocatalysis have been extensively explored, much remains to be accomplished, especially in the context of a truly sustainable protocols. Herein, we have developed an innovative strategy to produce a magnetic supported organocatalyst. This methodology includes the functionalization of $\gamma\text{-Fe}_2\text{O}_3@\text{SiO}_2$ with 3-aminopropyltriethoxysilane (APTES), aiming to obtain $\gamma\text{-Fe}_2\text{O}_3@\text{SiO}_2\text{-NH}_2$. Subsequently, a proline analogue was synthesized using a one-step procedure by post-modifying the $\gamma\text{-Fe}_2\text{O}_3@\text{SiO}_2\text{-NH}_2$ surface with penicillin G, which finally led to formation of an unprecedented proline analogue organocatalyst (Prn/ $\text{Fe}_2\text{O}_3@\text{SiO}_2$). In particular, this work has focused on penicillin G but it could be in principle extended to other proline derivatives. The obtained material was applied to the catalytic oxidation of isoeugenol and vanillyl alcohol and vanillin (Scheme 1).



Scheme 1. Schematic depiction of vanillin production from the different reactants in this work.

2. Results and Discussion

A magnetic-separable proline-based heterogeneous organocatalyst was successfully prepared following the protocol depicted in Figure 1. The unique properties of MNPs, which simplify the recovery of the material, together with the outstanding functionalities provides by the proline analogue, make $\text{Prn}/\text{Fe}_2\text{O}_3@\text{SiO}_2$ a potential candidate as catalyst in a broad range of reactions. An innovative protocol was designed for the in situ formation of a proline analogue on the surface of the aminofunctionalized $\gamma\text{-Fe}_2\text{O}_3@\text{SiO}_2$ by reaction with penicillin G. The latest molecule contains a four-membered β -lactam ring which can react with the amine group of $\gamma\text{-Fe}_2\text{O}_3@\text{SiO}_2\text{-NH}_2$. Consequently, a secondary amine adjacent to the carboxylate group was formed, corresponding to the proline analogue. Furthermore, the carboxylic acid group is formed from carboxylate to by proton exchange.

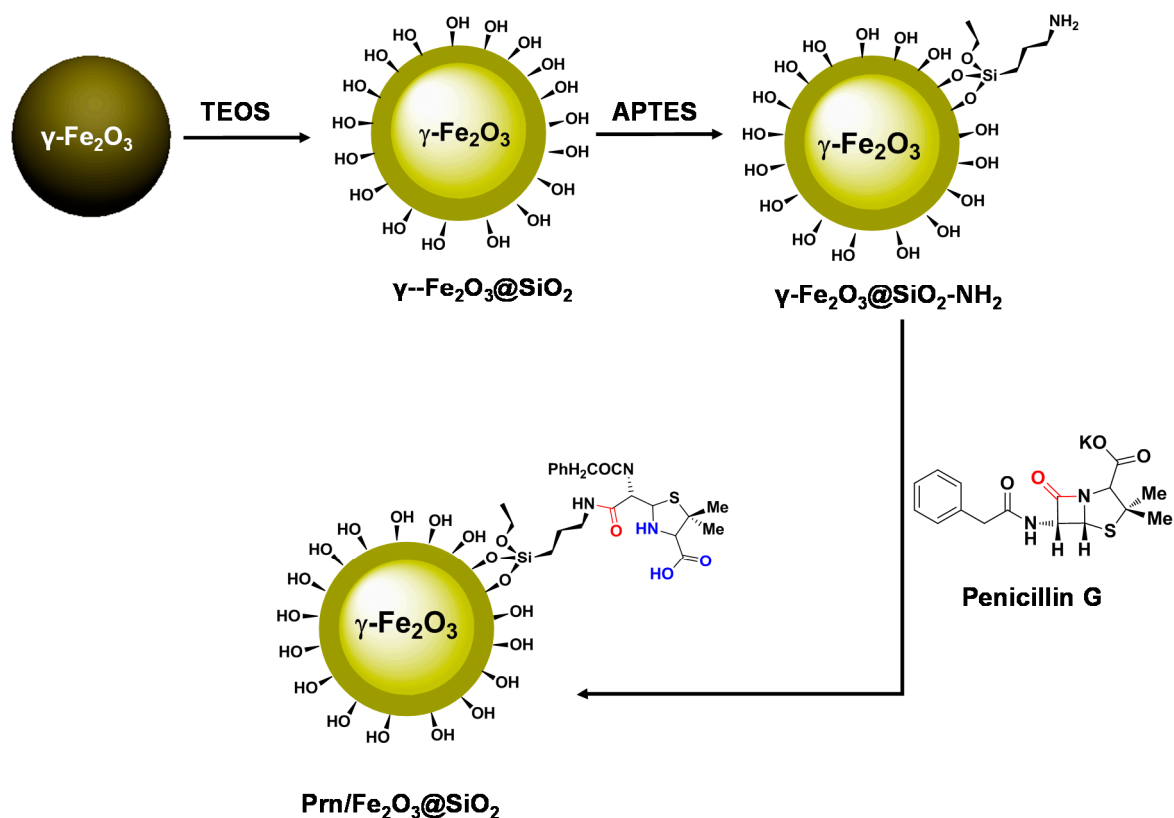


Figure 1. Overview of the preparation of $\text{Prn}/\text{Fe}_2\text{O}_3@\text{SiO}_2$ magnetic organocatalyst.

SEM image of $\text{Prn}/\text{Fe}_2\text{O}_3@\text{SiO}_2$ exhibited a homogeneous distribution with the formation of nanospherical particles (Figure 2a). This analysis displayed a certain tendency to form agglomerates, mostly associated with the magnetic properties of the obtained nanostructures. SEM analysis revealed a particle size average of 14.5 nm. As expected, EDS spectrum (Figure 2b) of $\text{Prn}/\text{Fe}_2\text{O}_3@\text{SiO}_2$ showed the presence of Si, O, N, C, S, and Fe, which is in accordance with SEM-mapping results (Figure 2e–j). Both EDS and SEM-mapping techniques corroborates the effective functionalization of the iron oxide MNPs and therefore confirmed that penicillin G successfully reacted with the amine group on the $\gamma\text{-Fe}_2\text{O}_3@\text{SiO}_2\text{-NH}_2$ surface, giving rise to the desired proline analogue. TEM analysis also confirmed the nanometric structure of $\text{Prn}/\text{Fe}_2\text{O}_3@\text{SiO}_2$ γ (Figure 2c), in good agreement with SEM results. Selected area electron diffraction (SAED) pattern of $\text{Prn}/\text{Fe}_2\text{O}_3@\text{SiO}_2$ (Figure 2d) revealed clear rings in accordance with the formation of crystalline gamma iron oxide [31].

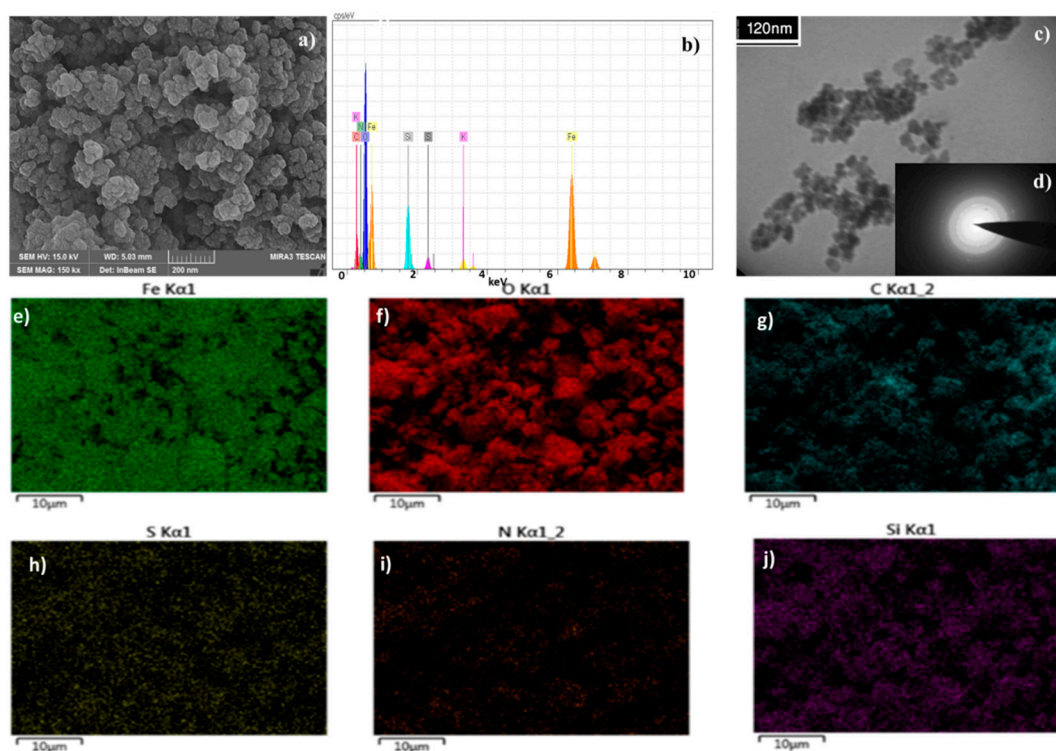


Figure 2. (a) SEM image, (b) EDS spectrum, (c) TEM image, and (d) SAED pattern of Prn/ Fe_2O_3 @ SiO_2 , (e–j) SEM elemental mapping of Prn/ Fe_2O_3 @ SiO_2 .

Thermal stability of Prn/ Fe_2O_3 @ SiO_2 was investigated by thermogravimetric analysis (Figure 3a). A progressive weight loss of 5 wt % was observed from 100 °C to 420 °C owing to the presence of unbounded/physisorbed water and solvents, and the possible dehydration of some silanol groups [32]. In addition, Figure 3a displayed a drastically drop of weight (12 wt %) at 420 °C. This decrease can be attributed to the degradation of organic moieties in the Prn/ Fe_2O_3 @ SiO_2 material. Moreover, DTA measurements displayed an exothermic band at 490 °C associated to the decomposition of the proline analogue.

The magnetic properties of the synthesized materials were investigated by VSM analysis (Figure 3b). The magnetization analysis of both, $\gamma\text{-Fe}_2\text{O}_3$ and Prn/ Fe_2O_3 @ SiO_2 samples confirmed their remarkably magnetic properties. The saturation magnetizations of $\gamma\text{-Fe}_2\text{O}_3$ and Prn/ Fe_2O_3 @ SiO_2 , resulted in similar values, 65 and 40 emu/g, respectively [33]. The slightly lower magnetization of the functionalized $\gamma\text{-Fe}_2\text{O}_3$ could be attributed to the proline analogue loading after functionalization. In any case, without a considerably loss of magnetism after the preparation process, Prn/ Fe_2O_3 @ SiO_2 features interesting properties of magnetic separation and manipulation in view of their potential catalytic applications.

X-ray diffraction analysis of $\gamma\text{-Fe}_2\text{O}_3$, $\gamma\text{-Fe}_2\text{O}_3$ @ SiO_2 - NH_2 , and Prn/ Fe_2O_3 @ SiO_2 materials was carried out and is reported in Figure 3c. The X-ray diffraction patterns of the three samples exhibited characteristic peaks, which matched well with standard $\gamma\text{-Fe}_2\text{O}_3$ reflections and revealed their highly crystalline nature [34]. After introducing amorphous SiO_2 , a small and expectable intensity decrease was observed. Nonetheless, these results suggest that after the functionalization process there is not considerable loss of crystallinity. Moreover, BET analysis (Figure 3d) showed a surface area of $75.2 \text{ m}^2\cdot\text{g}^{-1}$ and $53.1 \text{ m}^2\cdot\text{g}^{-1}$ for the $\gamma\text{-Fe}_2\text{O}_3$ and Prn/ Fe_2O_3 @ SiO_2 materials, respectively. Both products present a mesoporous structure, with a pore size of around 15 nm (Table 1).

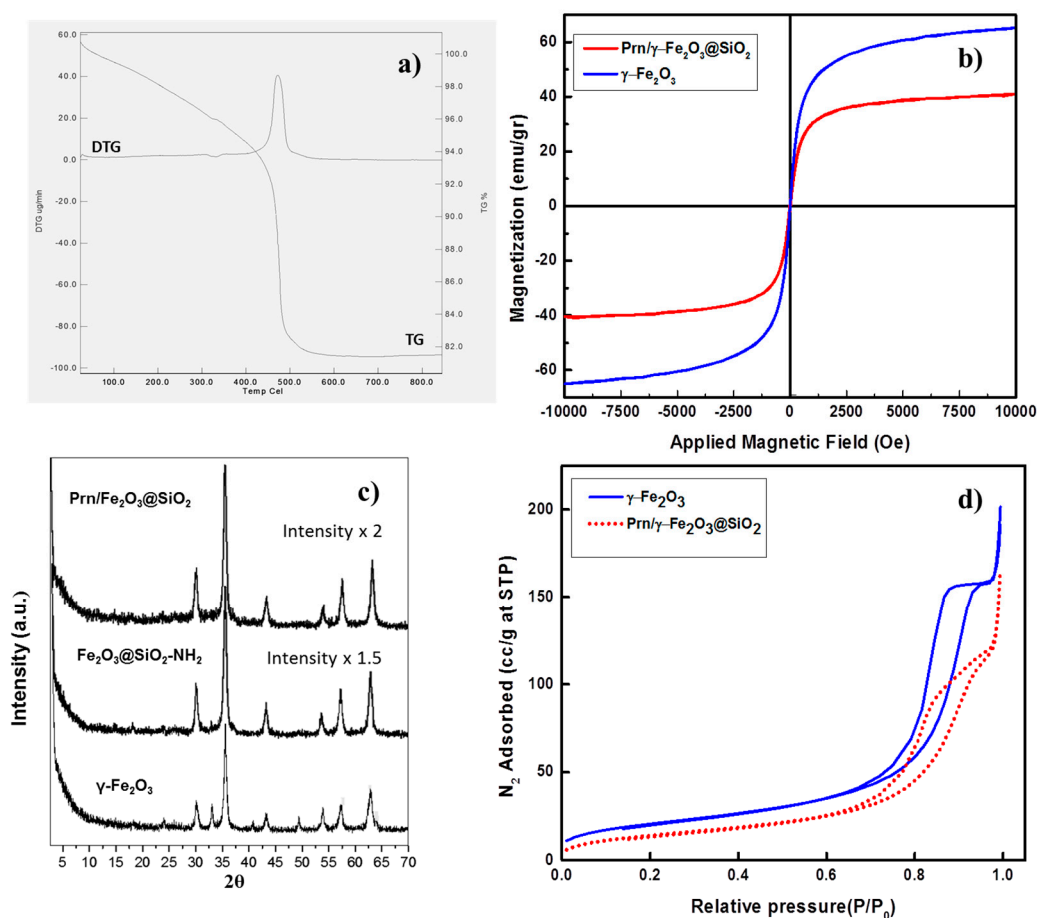


Figure 3. (a) Thermogravimetric (TG) and differential thermogravimetric (DTA) analyses of Prn/Fe₂O₃@SiO₂, (b) VSM diagram of γ-Fe₂O₃ and Prn/Fe₂O₃@SiO₂, (c) XRD pattern of γ-Fe₂O₃, γ-Fe₂O₃@SiO₂-NH₂ and Prn/Fe₂O₃@SiO₂, (d) N₂ physisorption isotherms of γ-Fe₂O₃ and Prn/Fe₂O₃@SiO₂.

Table 1. Textural properties.

Material	S _{BET} ^[a] (m ² g ^{−1})	D _{BJH} ^[b] (nm)	V _{BJH} ^[c] (cm ³ g ^{−1})
γ-Fe ₂ O ₃	75	14.5	0.27
Prn/Fe ₂ O ₃ @SiO ₂	53	15.2	0.2

^[a] S_{BET}: specific surface area was calculated by the Brunauer–Emmett–Teller (BET) equation. ^[b] D_{BJH}: mean pore size diameter was calculated by the Barret–Joyner–Halenda (BJH) equation. ^[c] V_{BJH}: pore volumes were calculated by the Barret–Joyner–Halenda (BJH) equation.

The effective functionalization of γ-Fe₂O₃@SiO₂ surface with penicillin-derived proline analogue was corroborated by FT-IR (Figure 4). This conclusion can be inferred from the appearance of a peak at 1644 cm^{−1}, related to the amide group formed by the reaction between penicillin G and amino groups on the γ-Fe₂O₃@SiO₂ surface. In addition, the band associated with carbonyl group in the lactam ring of pure penicillin (1174 cm^{−1}) [35] was absent in Prn/Fe₂O₃@SiO₂ spectrum, pointing to ring opening upon functionalization. Furthermore, a strong band at 1080 cm^{−1} was observed for both γ-Fe₂O₃@SiO₂ and Prn/Fe₂O₃@SiO₂ materials, corresponding to Si–O–Si stretching vibration. FT-IR spectra also showed several peaks in the 2900–3000 cm^{−1} wavenumber range, which can be assigned to C–H bonds in the aliphatic chains. Besides, characteristic transmission bands at 625 cm^{−1} and 550 cm^{−1} were associated with iron oxide [36].

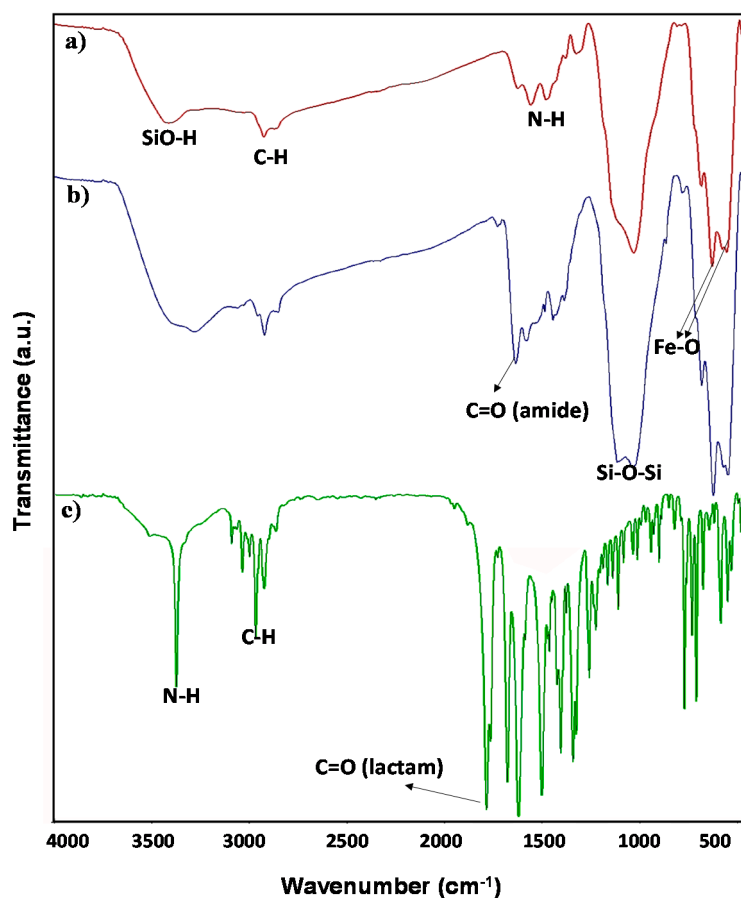


Figure 4. FT-IR spectra of (a) γ -Fe₂O₃@SiO₂-NH₂, (b) Prn/Fe₂O₃@SiO₂, and (c) penicillin G.

The catalytic activity of Prn/Fe₂O₃@SiO₂ was investigated in two reactions: (1) oxidation of isoeugenol and (2) vanillyl alcohol to vanillin. Firstly, the amount of catalyst was optimized to 20 mg of catalyst per each mmol of starting material. Subsequently, both reactions were studied using four oxidant agents: (a) hydrogen peroxide, (b) urea hydrogen peroxide (UHP), (c) *tert*-butyl hydroperoxide (*t*BHP), and (d) molecular oxygen. Although, the latest did not displayed satisfactory results, the other three oxidant agents resulted to be effective in this reaction, in particular, the best results were achieved using hydrogen peroxide. Moreover, the influence of the solvent on the effectiveness of the catalytic reaction was investigated using acetonitrile and toluene, the first one being the most appropriated. On the other hand, the effect of temperature was settled by performing the reaction at 80, 90, and 100 °C, establishing 90 °C as the most suitable temperature for the catalytic reaction (Table 2).

Under the model conditions, we monitored the reaction progress every 30 min. After 4 h, the reaction achieved the maximum conversion with a stable selectivity towards vanillin production. Compared to γ -Fe₂O₃ and catalyst-free reaction, Prn/Fe₂O₃@SiO₂ showed higher conversion and selectivity under similar conditions (Tables 3 and 4). The catalyst was also compared with its proton-unexchanged counterpart, for which a decrease in conversion for the latest material could be observed. These results indicated that the acidic nature, provided by the carboxylic group seems to have a crucial effect on the catalytic performance. In absence of the carboxylic acid, the amine group itself could promote the reaction. However, the oxidation reaction of isoeugenol, using the proton-unexchanged catalyst did not achieve a good catalytic activity towards vanillin production (Table 3). The presence of acidic species may be decisive in the catalytic conversion of isoeugenol to vanillin.

Table 2. Oxidation of vanillyl alcohol (A) and isoeugenol (B) to vanillin. (In bold: conditions for the best catalytic formance).

Vanillyl alcohol (A) 5 mmol $\xrightarrow{\text{Catalyst (0.1 g)}}$ Vanillin $\xleftarrow{\text{Catalyst (0.1 g)}}$ Isoeugenol (B) 5 mmol

Entry	Solvent	Oxidant	Time (h)	T (°C)	Conversion A (%)	Selectivity A (%)	Conversion B (%)	Selectivity B (%)
1	CH ₃ CN	-	15	90	traces	-	traces	-
2	CH ₃ CN	O ₂	15	90	25	92	13	32
3	CH ₃ CN	<i>t</i> BHP	4	90	65	88	33	43
4	CH ₃ CN	UHP	4	90	85	86	52	48
5	CH₃CN	H₂O₂	4	90	100	92	83	51
6	Toluene	H ₂ O ₂	10	90	88	88	60	42

Table 3. Catalytic oxidation of isoeugenol ^[a]. (In bold: best catalytic system).

Isoeugenol $\xrightarrow[\text{catalyst, 90 °C}]{\text{H}_2\text{O}_2, \text{CH}_3\text{CN}}$ Vanillin

Entry	Catalyst	Time (h)	Conversion (mol %)	Selectivity (mol %)		
				Vanillin	Diphenyl ether	Others ^[b]
1	Blank (no catalyst)	2	<15	7	84	<10
2	γ-Fe ₂ O ₃	2	49	44	15	<40
3	proton-unexchanged catalyst	2	21	14	-	<10
4	Prn/Fe₂O₃@SiO₂	2	65	55	<10	<40

^[a] Reaction conditions: 5 mmol isoeugenol, 1.2 mL H₂O₂, 8 mL acetonitrile, 0.1 g catalyst, 90 °C. ^[b] Oligomers and high molecular weight lignin-like compounds were detected as major reaction side products.

Table 4. Catalytic oxidation of vanillyl alcohol ^[a]. (In bold: best catalytic system).

Vanillyl alcohol $\xrightarrow[\text{catalyst, 90 °C}]{\text{H}_2\text{O}_2, \text{CH}_3\text{CN}}$ Vanillin

Entry	Catalyst	Time (h)	Conversion (mol %)	Selectivity Vanillin (mol %)
1	Blank (no cat.)	4	<10	>85
2	γ-Fe ₂ O ₃	4	60	90
3	proton-unexchanged catalyst	4	72	91
4	Prn/Fe₂O₃@SiO₂	4	>99	92

^[a] Reaction conditions: 5 mmol vanillyl alcohol, 1.2 mL H₂O₂, 8 mL acetonitrile, 0.1 g catalyst, 90 °C.

Reusability studies prove the high inherent stability and activity of Prn/Fe₂O₃@SiO₂ catalyst (Figure 5). For both reactions, the catalyst exhibited an excellent reusability for five consecutive cycles. Particularly, a drop in the activity of the catalyst after the fifth cycle was observed for isoeugenol conversion, which could be associated to the poisoning of the catalyst surface by side products of isoeugenol oxidation, in good agreement with the moderate selectivity observed to other products including lignin-like oligomers from vanillin oxidative polymerisation.

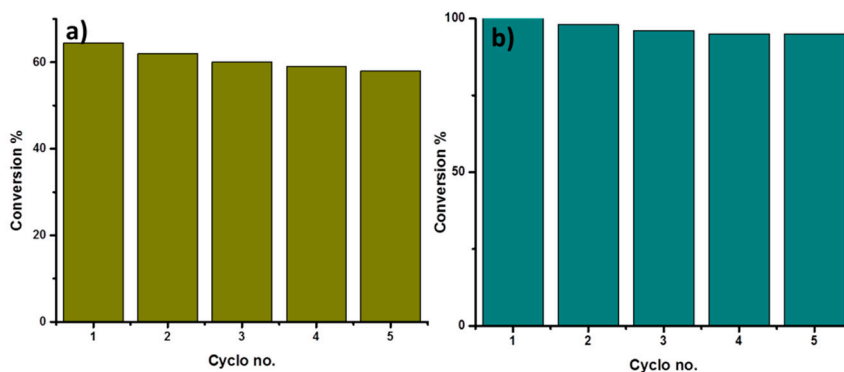


Figure 5. Reusability of the catalyst in conversion of the (a) isoeugenol and (b) vanillyl alcohol to vanillin under the optimal reaction conditions.

3. Materials and Methods

All chemicals were purchased from Sigma-Aldrich and used as received without further purification. Deionized (DI) water was used throughout this study. In order to characterize the synthesized materials, several techniques have been employed, including scanning electronic microscopy (SEM), electron dispersive spectroscopy (EDS) analysis, transmission electronic microscopy (TEM), selected area (electron) diffraction (SAED), thermogravimetric analysis (TGA), magnetization analysis, X-ray diffraction (XRD), N_2 physisorption, and Fourier transform infrared spectroscopy (FT-IR).

Electron dispersive spectra and SEM images were acquired using a Leo 1450vp scanning electron microscope equipped with a SC7620 energy dispersive spectrometer (Carl Zeiss AG, Oberkochen, Germany). TEM images were recorded in a Zeiss EM 900 microscope (Carl Zeiss AG, Oberkochen, Germany). Previously, the sample was dispersed in ethanol and transferred to a copper grid. Thermogravimetric analysis was accomplished using the System Setaram Setsys 12 TGA instrument (Setaram Instrumentation, Caluire, France), by heating the sample up to 800 °C at a rate of 10 °C·min^{−1} under N_2 flow. X-ray diffraction patterns were collected using the D8 Advanced Diffractometer (Bruker AXS, Billerica, MA, USA) with the Lynxeye detector at room temperature. FT-IR spectra were recorded on the ABB MB3000 infrared spectrophotometer (ABB, Zurich, Switzerland), equipped with an ATR PIKE MIRacle™ sampler, a window of ZnSe, and 256 scans at a resolution of 8 cm^{−1}.

The catalytic reactions were investigated by gas chromatography (GC) in an Agilent 6890N gas chromatograph (60 mL min^{−1} N_2 carrier flow, 20 psi column top head pressure) using a flame ionization detector (FID) (Agilent, Santa Clara, California, USA). The capillary column HP-5 (30 m × 0.32 mm × 0.25 mm) was employed. The conversion and selectivity were calculated from the chromatograms by

$$\text{Conversion}(\%) = \frac{[C_{\text{Initial}} - C_{\text{Final}}]}{C_{\text{Initial}}} \times 100$$

$$\text{Selectivity}(\%) = \frac{C_{\text{Product}}}{[C_{\text{Initial}} - C_{\text{Final}}]} \times 100$$

where C_{Initial} and C_{Final} are the concentrations of the reagents before and after the reaction, respectively. C_{Product} is the concentration of the product.

3.1. Synthesis of $\gamma\text{-Fe}_2\text{O}_3\text{@SiO}_2$

Synthesis of $\gamma\text{-Fe}_2\text{O}_3$ was carried out employing a reported chemical co-precipitation protocol with a slight modification [37,38]. Accordingly, $\text{FeCl}_2 \cdot 4\text{H}_2\text{O}$ (0.495 g) and $\text{FeCl}_3 \cdot 6\text{H}_2\text{O}$ (1.35 g) were first dissolved in acetic acid (3 wt %, 100 mL) and stirred at room temperature. Subsequently, a NH_4OH solution (0.7 M, 50 mL) was added to the mixture at room temperature to reach a pH value of 12.

After 15 min, a black precipitate was observed. The obtained solid was collected by an external magnet, washed three times with a mixture water/ethanol (1:1) and dried at 100 °C for 12 h. Finally, the material was calcined at 300 °C for 3 h. The obtained $\gamma\text{-Fe}_2\text{O}_3$ (1 g) was dispersed in ethanol (40 mL) and sonicated for 30 min at room temperature. Afterward, TEOS (5 mL) was added dropwise and the mixture was stirred at 40 °C for 24 h. The final core-shell nanostructure was collected by an external magnet, washed three times with ethanol and dried at 80 °C under vacuum for 6 h to obtain a $\gamma\text{-Fe}_2\text{O}_3@\text{SiO}_2$ nanomaterial.

3.2. Synthesis of Prn/ $\gamma\text{-Fe}_2\text{O}_3@\text{SiO}_2$

The obtained $\gamma\text{-Fe}_2\text{O}_3@\text{SiO}_2$ (2.0 g) was dispersed in dry toluene (20 mL) and sonicated for 45 min. Then, APTES (0.5 mL) was added to the dispersion and slowly heated up to 105 °C. The reaction mixture was stirred for 24 h under reflux conditions. The resulted amino-functionalized material ($\gamma\text{-Fe}_2\text{O}_3@\text{SiO}_2\text{-NH}_2$) was redispersed in 20 mL of distilled water and thereafter, a solution of penicillin G potassium salt (1 g) in ethanol:water (1:1, 10 mL) was added to the dispersion. The reaction mixture was stirred for 48 h at 60 °C. The obtained material was washed several times with ethanol and oven-dried at 60 °C for 5 h. In addition, the product was redispersed in a dilute HCl solution (pH = 4.5) and stirred for 6 h. Finally, the synthesized Prn/ $\gamma\text{-Fe}_2\text{O}_3@\text{SiO}_2$ was washed with distilled water and dried at 100 °C in a vacuum oven.

3.3. Catalytic Experiments

The oxidation of isoeugenol to vanillin was performed using 0.8 mL of isoeugenol, 1.2 mL of H_2O_2 , 8 mL of acetonitrile (CH_3CN), and 0.1 g of the previously synthesized organocatalyst (0.01 g/mL). The reaction mixture was stirred at 90 °C for 24 h by using a multiple parallel synthesis system (Carrusel Reaction Station, Radleys Discovery Technologies Ltd., Saffron Walden, UK). During the reaction, samples were taken every 30 min and characterized by gas chromatography. The oxidation of vanillyl alcohol was carried out employing the same procedure.

4. Conclusions

In summary, an unprecedented proline analogue was generated in situ from the reaction between penicillin G and the amino-functionalized surface of $\gamma\text{-Fe}_2\text{O}_3@\text{SiO}_2$. The magnetic $\gamma\text{-Fe}_2\text{O}_3@\text{SiO}_2$ core shell structure facilitated the recovery and reusability of the resulted organocatalyst. The obtained material was applied to the conversion of vanillyl alcohol and isoeugenol to vanillin. The presence of acidic functionalities in the catalyst was decisive for the isoeugenol oxidation. In both reactions, the acidic and basic sites of the Prn/ $\gamma\text{-Fe}_2\text{O}_3@\text{SiO}_2$, exhibiting a synergic effect, enhancing the catalytic efficiency towards higher conversion and selectivity.

Acknowledgments: Farveh Saberi gratefully acknowledges Sistan and Baluchestan University of Iran for the financial support of the research as well as Iran Nanotechnology Initiative Council for complementary supports. The publication has been prepared with support from RUDN University Program 5-100.

Author Contributions: Rafael Luque, Farveh Saberi and Araceli Garcia conceived and designed the experiments; Farveh Saberi and Daily Rodríguez-Padrón performed the experiments; Rafael Luque, Farveh Saberi and Hamid Reza Shaterian analyzed the data; Rafael Luque and Hamid Reza Shaterian contributed with reagents/materials/analysis tools for all experiments; Farveh Saberi and Daily Rodríguez-Padrón wrote the paper.

Conflicts of Interest: The authors declare no conflict of interest.

References

1. Gusevskaya, E.V.; Menini, L.; Parreira, L.A.; Mesquita, R.A.; Kozlov, Y.N.; Shulpin, G.B. Oxidation of isoeugenol to vanillin by the “ H_2O_2 –vanadate–pyrazine-2-carboxylic acid. *J. Mol. Catal. A Chem.* **2012**, 363–364, 140–147. [[CrossRef](#)]

2. Huang, W.-B.; Du, C.-Y.; Jiang, J.-A.; Ji, Y.-F. Concurrent synthesis of vanillin and isovanillin. *Res. Chem. Intermed.* **2013**, *39*, 2849–2856. [[CrossRef](#)]
3. Lampman, G.M.; Sharpe, S.D. A phase transfer catalyzed permanganate oxidation: Preparation of vanillin from isoeugenol acetate. *J. Chem. Educ.* **1983**, *60*, 503. [[CrossRef](#)]
4. Franco, A.; De, S.; Balu, A.M.; Romero, A.A.; Luque, R. Selective Oxidation of Isoeugenol to Vanillin over Mechanochemically Synthesized Aluminosilicate Supported Transition Metal Catalysts. *ChemistrySelect* **2017**, *2*, 9546–9551. [[CrossRef](#)]
5. Filiciotto, L.; Balu, A.M.; Romero, A.A.; Rodríguez-Castellón, E.; van der Waal, J.C.; Luque, R. Benign-by-design preparation of humin-based iron oxide catalytic nanocomposites. *Green Chem.* **2017**, *19*, 4423–4434. [[CrossRef](#)]
6. Adilina, I.B.; Hara, T.; Ichikuni, N.; Shimazu, S. Oxidative cleavage of isoeugenol to vanillin under molecular oxygen catalysed by cobalt porphyrin intercalated into lithium taeniolite clay. *J. Mol. Catal. A* **2012**, *361*, 72–79. [[CrossRef](#)]
7. Behling, R.; Valange, S.; Chatel, G. Heterogeneous catalytic oxidation for lignin valorization into valuable chemicals: What results? What limitations? What trends? *Green Chem.* **2016**, *18*, 1839–1854. [[CrossRef](#)]
8. Behera, G.C.; Parida, K. Liquid phase catalytic oxidation of benzyl alcohol to benzaldehyde over vanadium phosphate catalyst. *Appl. Catal. A* **2012**, *413*, 245–253. [[CrossRef](#)]
9. Marquez-Medina, M.D.; Prinsen, P.; Li, H.; Shih, K.; Romero, A.A.; Luque, R. Continuous-Flow Synthesis of Supported Magnetic Iron Oxide Nanoparticles for Efficient Isoeugenol Conversion into Vanillin. *ChemSusChem* **2018**, *11*, 389–396. [[CrossRef](#)] [[PubMed](#)]
10. Watson, S.; Beydoun, D.; Amal, R. Synthesis of a novel magnetic photocatalyst by direct deposition of nanosized TiO₂ crystals onto a magnetic core. *J. Photochem. Photobiol. A* **2002**, *148*, 303–313. [[CrossRef](#)]
11. Polshettiwar, V.; Luque, R.; Fihri, A.; Zhu, H.; Bouhrara, M.; Basset, J.-M. Magnetically recoverable nanocatalysts. *Chem. Rev.* **2011**, *111*, 3036–3075. [[CrossRef](#)] [[PubMed](#)]
12. Rodríguez-Padrón, D.; Jodlowski, A.D.; de Miguel, G.; Puente-Santiago, A.R.; Balu, A.M.; Luque, R. Synthesis of carbon-based fluorescent polymers driven by catalytically active magnetic bioconjugates. *Green Chem.* **2018**, *20*, 225–229. [[CrossRef](#)]
13. Lu, A.H.; Salabas, E.E.L.; Schüth, F. Magnetic nanoparticles: Synthesis, protection, functionalization, and application. *Angew. Chem. Int. Ed.* **2007**, *46*, 1222–1244. [[CrossRef](#)] [[PubMed](#)]
14. Doustkhah, E.; Rostamnia, S.; Gholipour, B.; Zeynizadeh, B.; Baghban, A.; Luque, R. Design of chitosan-dithiocarbamate magnetically separable catalytic nanocomposites for greener aqueous oxidations at room temperature. *Mol. Catal.* **2017**, *434*, 7–15. [[CrossRef](#)]
15. Kuhn, L.T.; Bojesen, A.; Timmermann, L.; Nielsen, M.M.; Mørup, S. Structural and magnetic properties of core-shell iron-iron oxide nanoparticles. *J. Phys. Condens. Matter* **2002**, *14*, 13551. [[CrossRef](#)]
16. Rafiee, E.; Eavani, S. H₃PW₁₂O₄₀ supported on silica-encapsulated γ -Fe₂O₃ nanoparticles: A novel magnetically-recoverable catalyst for three-component Mannich-type reactions in water. *Green Chem.* **2011**, *13*, 2116–2122. [[CrossRef](#)]
17. Khalafi-Nezhad, A.; Divar, M.; Panahi, F. Magnetic nanoparticles-supported tungstic acid (MNP-TA): An efficient magnetic recyclable catalyst for the one-pot synthesis of spirooxindoles in water. *RSC Adv.* **2015**, *5*, 2223–2230. [[CrossRef](#)]
18. Riente, P.; Mendoza, C.; Pericás, M.A. Functionalization of Fe₃O₄ magnetic nanoparticles for organocatalytic Michael reactions. *J. Mater. Chem.* **2011**, *21*, 7350–7355. [[CrossRef](#)]
19. Doustkhah, E.; Rostamnia, S.; Imura, M.; Ide, Y.; Mohammadi, S.; Hyland, C.J.; You, J.; Tsunoji, N.; Zeynizadeh, B.; Yamauchi, Y. Thiourea bridged periodic mesoporous organosilica with ultra-small Pd nanoparticles for coupling reactions. *RSC Adv.* **2017**, *7*, 56306–56310. [[CrossRef](#)]
20. Rostamnia, S.; Doustkhah, E. Nanoporous silica-supported organocatalyst: A heterogeneous and green hybrid catalyst for organic transformations. *RSC Adv.* **2014**, *4*, 28238–28248. [[CrossRef](#)]
21. Polshettiwar, V.; Baruwati, B.; Varma, R.S. Magnetic nanoparticle-supported glutathione: A conceptually sustainable organocatalyst. *Chem. Commun.* **2009**, 1837–1839. [[CrossRef](#)] [[PubMed](#)]
22. Rostamnia, S.; Doustkhah, E. Increased SBA-15-SO₃H catalytic activity through hydrophilic/hydrophobic fluoroalkyl-chained alcohols (RFOH/SBA-15-Pr-SO₃H). *Synlett* **2015**, *26*, 1345–1347. [[CrossRef](#)]

23. Rodríguez-Padrón, D.; Balu, A.M.; Romero, A.A.; Luque, R. New bio-nanocomposites based on iron oxides and polysaccharides, applied to oxidation and alkylation reactions. *Beilstein J. Org. Chem.* **2017**, *13*, 1982–1993. [[CrossRef](#)] [[PubMed](#)]
24. Yang, H.; Li, S.; Wang, X.; Zhang, F.; Zhong, X.; Dong, Z.; Ma, J. Core-shell silica magnetic microspheres supported proline as a recyclable organocatalyst for the asymmetric aldol reaction. *J. Mol. Catal. A* **2012**, *363*, 404–410. [[CrossRef](#)]
25. Yang, G.; Zhou, L. Mechanisms and reactivity differences of proline-mediated catalysis in water and organic solvents. *Catal. Sci. Technol.* **2016**, *6*, 3378–3385. [[CrossRef](#)]
26. Bhattacharjee, D.; Sutradhar, D.; Chandra, A.K.; Myrboh, B. L-proline as an efficient asymmetric induction catalyst in the synthesis of chromeno[2,3-*d*]pyrimidine-triones, xanthenes in water. *Tetrahedron* **2017**, *73*, 3497–3504. [[CrossRef](#)]
27. Akceylan, E.; Uyanik, A.; Eymur, S.; Sahin, O.; Yilmaz, M. Calixarene-proline functionalized iron oxide magnetite nanoparticles (Calix-Pro-MN): An efficient recyclable organocatalyst for asymmetric aldol reaction in water. *Appl. Catal. A* **2015**, *499*, 205–212. [[CrossRef](#)]
28. Zhang, H.; Han, M.; Chen, T.; Xu, L.; Yu, L. Poly (*N*-isopropylacrylamide-co-L-proline)-catalyzed Claisen–Schmidt and Knoevenagel condensations: Unexpected enhanced catalytic activity of the polymer catalyst. *RSC Adv.* **2017**, *7*, 48214–48221. [[CrossRef](#)]
29. Aghahosseini, H.; Ramazani, A.; Ślepokura, K.; Lis, T. The first protection-free synthesis of magnetic bifunctional L-proline as a highly active and versatile artificial enzyme: Synthesis of imidazole derivatives. *J. Colloid Interface Sci.* **2018**, *511*, 222–232. [[CrossRef](#)] [[PubMed](#)]
30. Khalafi-Nezhad, A.; Shahidzadeh, E.S.; Sarikhani, S.; Panahi, F. A new silica-supported organocatalyst based on L-proline: An efficient heterogeneous catalyst for one-pot synthesis of spiroindolones in water. *J. Mol. Catal. A* **2013**, *379*, 1–8. [[CrossRef](#)]
31. Lee, S.; Shin, K.Y.; Jang, J. Enhanced magnetorheological performance of highly uniform magnetic carbon nanoparticles. *Nanoscale* **2015**, *7*, 9646–9654. [[CrossRef](#)] [[PubMed](#)]
32. Yepez, A.; Hidalgo, J.M.; Pineda, A.; Černý, R.; Jiša, P.; Garcia, A.; Luque, R. Mechanistic insights into the hydroconversion of cinnamaldehyde using mechanochemically-synthesized Pd/Al-SBA-15 catalysts. *Green Chem.* **2015**, *17*, 565–572. [[CrossRef](#)]
33. Rajpure, K.Y. Exploring structural and magnetic properties of nanocrystalline iron oxide synthesized by autocombustion method. *Superlattices Microstruct.* **2015**, *77*, 181–195. [[CrossRef](#)]
34. Hyeon, T.; Lee, S.S.; Park, J.; Chung, Y.; Na, H.B. Synthesis of highly crystalline and monodisperse maghemite nanocrystallites without a size-selection process. *J. Am. Chem. Soc.* **2001**, *123*, 12798–12801. [[CrossRef](#)] [[PubMed](#)]
35. Choudhury, A.J.; Gogoi, D.; Kandimalla, R.; Kalita, S.; Chaudhari, Y.B.; Khan, M.R.; Chutia, J. Penicillin impregnation on oxygen plasma surface functionalized chitosan/*Antheraea assama* silk fibroin: Studies of antibacterial activity and antithrombogenic property. *Mater. Sci. Eng. C* **2016**, *60*, 475–484. [[CrossRef](#)] [[PubMed](#)]
36. Ismail, R.A.; Sulaiman, G.M.; Abdulrahman, S.A.; Marzoog, T.R. Antibacterial activity of magnetic iron oxide nanoparticles synthesized by laser ablation in liquid. *Mater. Sci. Eng. C* **2015**, *53*, 286–297. [[CrossRef](#)] [[PubMed](#)]
37. Azizi, K.; Heydari, A. Vitamin B1 supported on silica-encapsulated γ -Fe₂O₃ nanoparticles: Design, characterization and application as a greener biocatalyst for highly efficient acylation. *RSC Adv.* **2014**, *4*, 8812–8816. [[CrossRef](#)]
38. Sobhani, S.; Ghasemzadeh, M.S.; Honarmand, M. Piperidine and piperazine immobilized on iron oxide nanoparticles as magnetically recyclable heterogeneous catalysts for one-pot synthesis of β -phosphonomalonates. *Catal. Lett.* **2014**, *144*, 1515–1523. [[CrossRef](#)]

